ADVANCED MATERIALS
www.advmat.de

Antigen-Directed Fabrication of a Multifunctional Nanovaccine with Ultrahigh Antigen Loading Efficiency for Tumor Photothermal-Immunotherapy

Jinbin Pan, Yaqiong Wang, Cai Zhang, Xiaoyi Wang, Haoyu Wang, Jiaojiao Wang, Yizhong Yuan, Xu Wang, Xuejun Zhang, Chunshui Yu, Shao-Kai Sun, and Xiu-Ping Yan*

Current antigen-encapsulated multifunctional nanovaccines for oncotherapy suffer from limited antigen loading efficiency, low yield, tedious manufacture, and systemic toxicity. Here, an antigen-directed strategy for the fabrication of multifunctional nanovaccine with ultrahigh antigen loading efficiency in a facile way for tumor photothermal-immunotherapy is shown. As a proof of concept, a model antigen ovalbumin (OVA) is used as a natural carrier to load a representative theranostic agent indocyanine green (ICG). Mixing OVA and ICG in aqueous solution gives the simplest multifunctional nanovaccine so far. The nanovaccine owns antigen loading efficiency of 80.8%, high yield of >90%, intense near-infrared absorption and fluorescence, excellent reproducibility, good aqueous solubility and stability, and favorable biocompatibility. These merits not only guarantee sensitive labeling/tracking and efficient stimulation of dendritic cells, but also reliable imaging-guided photothermal-immunotherapy of tumors and tumor prevention. The proposed strategy provides a facile and robust method for large-scale and reproducible fabrication of multifunctional nanovaccines with ultrahigh antigen loading efficiency for tumor therapy.

Early screening and advanced clinical treatments, such as surgery, chemotherapy, and radiotherapy, have significantly reduced the mortality of cancer.[1] However, incredible heterogeneity of tumors makes efficient tumor therapy fundamentally difficult.[2] Immunotherapy, which trains and stimulates the immune system of body itself to detect and eliminate tumors, is emerging as a new generation of cancer therapy, and shows promising potential in altering the cancer treatment paradigm.[3] Cancer nanovaccine-based immunotherapy has received great attention recently as nanovaccines, not only triggering antigen-specific immunities, but also providing a long-term immune-memory effect.[4]

Current strategies for the fabrication of nanovaccines mainly employ various nanocarriers, such as liposome,[5] polymer,[6] inorganic nanoparticles,[7] biopolymer implant,[8] hydrogel,[9] scaffold,[10] and biomimetic bacteria[11] as depots for controlled release of antigen, adjuvants, and cytokines. However, their limited antigen loading efficiency, low yield, tedious manufacturing process, and systemic toxicity seriously hinder clinical benefits

Dr. J. Pan, Y. Wang, Dr. H. Wang, Prof. C. Yu
Department of Radiology
Tianjin Key Laboratory of Functional Imaging
Tianjin Medical University
Tianjin 300052, China

C. Zhang
College of Chemistry
Research Center for Analytical Sciences
State Key Laboratory of Medicinal Chemical Biology
and Tianjin Key Laboratory of Molecular Recognition and Biosensing
Nankai University
Tianjin 300071, China

X. Wang
Department of Ultrasound
The Second Hospital of Tianjin Medical University
Tianjin 300211, China

The ORCID identification number(s) for the author(s) of this article can be found under https://doi.org/10.1002/adma.201704408.

DOI: 10.1002/adma.201704408

J. Wang, Y. Yuan, Prof. X. Zhang, Dr. S.-K. Sun
School of Medical Imaging
Tianjin Medical University
Tianjin 300203, China
E-mail: shaokaisun@163.com

Dr. X. Wang
Tianjin Key Laboratory on Technologies Enabling Development
of Clinical Therapeutics and Diagnostics (Theranostics)
School of Pharmacy
Tianjin Medical University
Tianjin 300070, China

Prof. X.-P. Yan
State Key Laboratory of Food Science and Technology
Institute of Analytical Foodsafetiology
School of Food Science and Technology
Jiangnan University
Wuxi 214122, China

Prof. X.-P. Yan
Collaborative Innovation Center of Chemical Science
and Engineering (Tianjin)
Tianjin 300071, China

of immunotherapy.[12] Ideally, nanovaccines are easily produced in aqueous solution under mild conditions, and exhibit high antigen loading efficiency, high yield, excellent reproducibility, favorable biocompatibility, and powerful immune response.[13] Nevertheless, it is still challenging to develop creative strategies for fabrication of such ideal nanovaccines.

Nanovaccine-based immunotherapy is capable of controlling residual tumors and inducing long-term tumor resistance by arousing a systemic antitumor immunity, but hard to eradicate primary tumors.[12b] Integration of nanovaccine-based immunotherapy and other complementary therapies makes it possible to achieve synergistic therapy against various morphologies of tumors.[14] Photothermal therapy, which employs photoabsorbers to generate heat from near-infrared (NIR) light energy for tumor ablation, provides a robust therapeutic efficacy in the treatment of primary tumors in a short-time therapeutic manner.[15] Therefore, construction of multifunctional nanovaccines combining immunotherapy with photothermal therapy offers promising opportunities for the synergistic treatment of tumors with various morphologies.[16] Besides, involvement of imaging modality in multifunctional nanovaccines allows dendritic cell (DC) labeling/tracking and imaging-guided multiple therapies, further remarkably enhancing the theranostic efficacy.

Protein-mediated synthesis of multifunctional nanostructures with fascinating features has received tremendous attention due to its high efficiency and mild synthesis conditions.[17] Various nanoagents with great clinical translation potential have been fabricated by mimicking biomineralization and utilizing noncovalent interactions using proteins as templates or carriers and extensively applied in imaging and therapy of tumors.[18] Inspiringly, antigens, a type of special proteins, show great potential to serve as natural carriers for the loading of various theranostic agents to generate multifunctional nanovaccines with ultrahigh loading of antigen. Therefore, it is significant to construct a multifunctional nanovaccine with ideal features using antigen itself as the carrier in a facile way.

Herein, we report a facile antigen-directed strategy for the fabrication of a multifunctional nanovaccine with ultrahigh antigen loading efficiency for tumor photothermal-immunotherapy (**Figure 1**). As a proof of concept, the nanovaccine was constructed via simple mixing of ovalbumin (OVA), a model antigen, and indocyanine green (ICG), a representative theranostic reagent in aqueous solution at room temperature. There is no need for any toxic reagents, severe conditions, and inert gas protection for synthesis. ICG is the only Food and Drug Administration-approved NIR fluorescent dye in clinic and endows the prepared OVA–ICG nanovaccine with NIR fluorescent imaging and photothermal therapy abilities.[18f] The prepared OVA–ICG nanovaccine owns antigen loading efficiency of 80.8%, high yield (>90%), intense NIR absorption and fluorescence, excellent reproducibility, admirable aqueous solubility/stability, and favorable biocompatibility. The robust multifunctional nanovaccine enables high-efficient stimulation and sensitive labeling/tracking of dendritic cells, and allows imaging-guided photothermal therapy and immunotherapy for different morphologies of tumors in vivo. Additionally, the OVA–ICG nanovaccine provides a robust tumor prevention effect and makes the immunized mice possess an impressing tumor suppression capability toward transplanted tumors. To the best of our knowledge, it is the first time that an antigen-directed strategy for building nanovaccines is proposed, and the

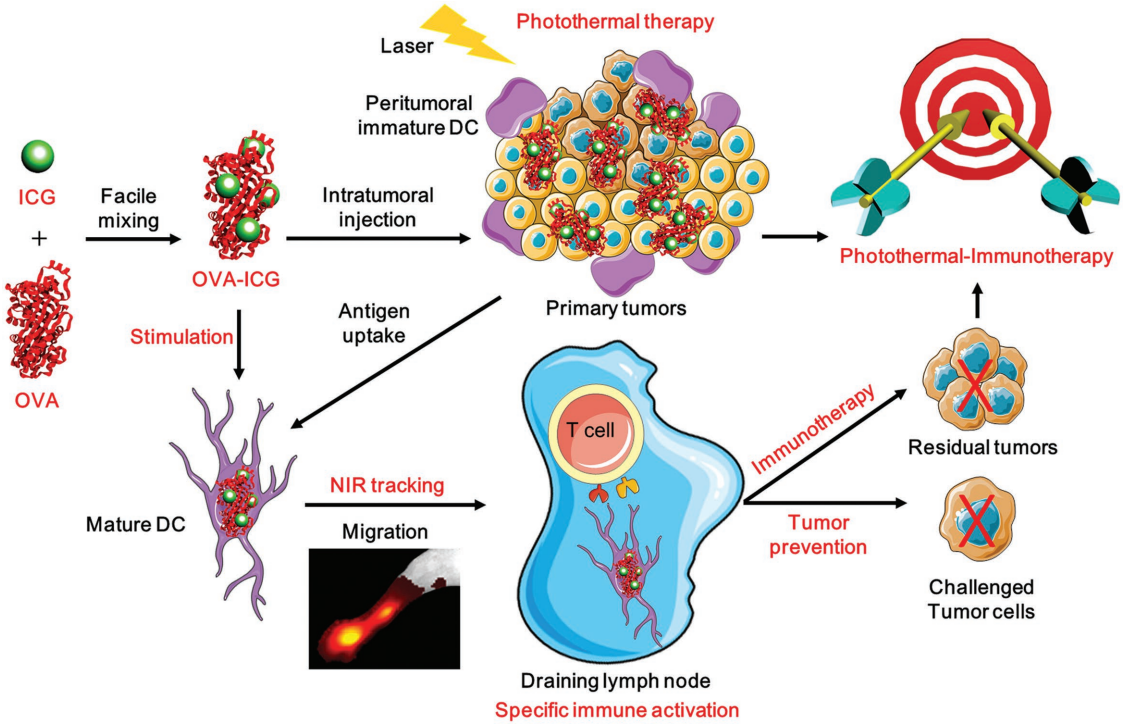

Figure 1. Illustration for fabrication and mechanism of OVA–ICG nanovaccine for photothermal-immunotherapy against tumor, DC stimulation/tracking, and tumor prevention.

model OVA–ICG nanoassembly is the simplest multifunctional nanovaccine so far.

The OVA–ICG nanovaccine was fabricated at room temperature via an extremely facile and green mixing method (Figure 1). Amphiphilic ICG effortlessly attaches to OVA to generate the OVA–ICG nanoassembly based on noncovalent interactions. The interaction between OVA and ICG was investigated by fluorescent spectrometry. The fluorescence emission spectra of OVA solutions containing different concentrations of ICG (0×10^{-6}–20×10^{-6} M) were recorded by excited at 280 nm at different temperatures (T = 293 and 303 K) (Figures S1 and S2, Supporting Information). OVA exhibits a strong fluorescence emission at 343 nm due to its tryptophan residues, and increased ICG induced remarkable fluorescence quenching due to the interaction of OVA and ICG. The bimolecular quenching constant K_q was calculated according to the Stern–Volmer equation. The value of K_q (1.94×10^{12} L mol^{-1} s^{-1} at 293 K) is much larger than the maximum scatter collision quenching constant of various quenchers with the biopolymer (2×10^{10} L mol^{-1} s^{-1}), illustrating the static quenching mechanism of OVA induced by ICG.[19] The binding constant (K_a) and thermodynamic parameters of OVA–ICG system were also calculated. K_a was determined to be 6.7×10^3 L mol^{-1} (at 293 K), ensuring the formation of stable OVA–ICG complex. The negative values of ΔG revealed that the interaction process between OVA and ICG is spontaneous. The fluorescent spectrometry analysis illustrates the binding ability and thermodynamic parameter for the formation of OVA-ICG complex.[19] Therefore, the efficient noncovalent interactions ensured the formation of OVA–ICG nanoassembly under mild conditions.

The as-prepared OVA–ICG nanovaccine owned a spherical-like geometry with a diameter of about 14.7 nm from high-resolution transmission electron microscopy (HRTEM) image (**Figure 2**a). The hydrodynamic diameter of OVA–ICG nanovaccine was measured to be 31.2 nm with dynamic light scattering (Figure S3, Supporting Information), which was larger than free OVA. The zeta potential of OVA–ICG (–28.6 mV) is approximate with OVA (–31.7 mV). No significant changes of hydrodynamic sizes and particle dispersion index for both the OVA–ICG and OVA aqueous solutions were observed during the 7 d monitoring (Figures S4 and S5, Supporting Information), demonstrating the good colloidal stability of OVA–ICG nanovaccine. The characteristic Fourier transform infrared (FTIR) absorption bands of −OH (3291 cm^{-1}), amide I (1651 cm^{-1}), and amide II (1531 cm^{-1}) confirm the presence of OVA in OVA–ICG nanovaccine (Figure 2b). The loading of ICG endows OVA–ICG with remarkable NIR absorption at 779 nm and intense NIR fluorescent emission at 820 nm (Figure 2c,d), guaranteeing its good photothermal conversion efficiency and sensitive NIR fluorescent imaging capability. The contents of ICG and OVA in the OVA–ICG nanovaccine were 19.2% and 80.8%, respectively. The ultrahigh antigen loading efficiency makes the nanovaccine possible with strong immunotherapy efficacy induced by low dose of administration. The strong NIR absorption of ICG in the nanovaccine enables its outstanding photothermal performance. 808 nm laser irradiation with different power densities made the temperature of OVA–ICG solution more rapidly increase in a concentration-dependent manner than pure water (Figure 2e,f and Figure S6 (Supporting Information)). Pure ICG solution and OVA–ICG solution with the same concentration of ICG exhibited similar temperature

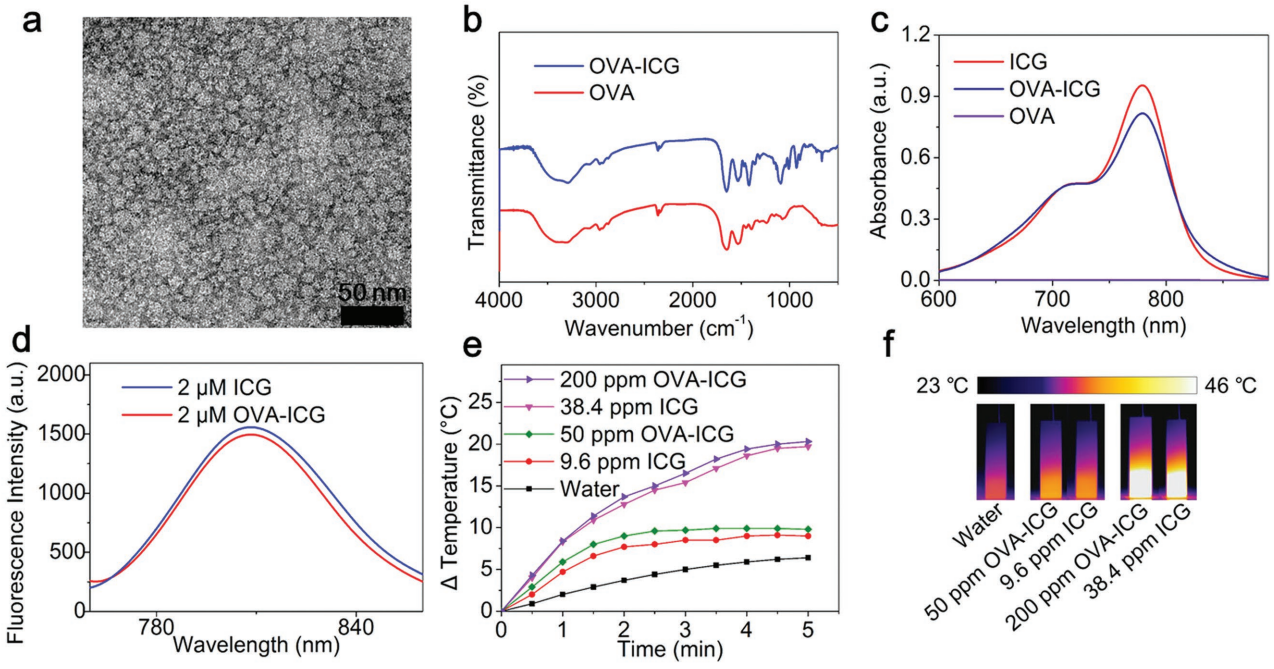

Figure 2. Characterizations and photothermal performance of OVA–ICG nanovaccine. a) HRTEM image of OVA–ICG with negative staining using sodium phosphotungstate. b) FTIR spectra of OVA and OVA–ICG. c) UV–vis–NIR spectra of OVA, ICG, and OVA–ICG. d) Fluorescence spectra of ICG and OVA–ICG with same concentration of ICG. e) Temperature rising curves for different solutions under the irradiation of 808 nm laser (2.0 W cm^{-2}, 5 min). f) IR images of different solutions under the irradiation of 808 nm laser (2.0 W cm^{-2}, 5 min).

enhancement under the same irradiation conditions, indicating that the OVA–ICG nanovaccine retained the photothermal effect of ICG. The results show that OVA–ICG nanovaccine still has good photothermal performance.

Furthermore, the obtained OVA–ICG nanovaccine can be conveniently lyophilized for a long-term storage in powder. The nanovaccine powder can be easily redispersed in various media including water, phosphate buffered saline solution (PBS), normal saline, cell culture media, and fetal bovine serum with a good long-term colloidal stability (at least 14 d). In contrast, pure ICG possessed relatively poor colloidal stability in the same media, especially in normal saline, and began to precipitate after a long-time storage (Figure S7, Supporting Information). These results indicated the integration of OVA and ICG effectively improves the colloidal stability of ICG. Moreover, the photostability of ICG was also remarkably improved after stabilization of OVA, and fluorescence decrease of OVA–ICG solution (20%) was much lower than that of pure ICG solution (50%) after storing in dark for a week. The enhanced photostability benefits long-term cell labeling and tracking using the OVA–ICG nanovaccine.

The cytotoxicity of OVA–ICG nanovaccine was evaluated via a standard methyl thiazolyl tetrazolium (MTT) test with both B16 cells (overexpressing OVA) and DC 2.4 cells (a recognized immature dendritic cell line). OVA–ICG nanovaccine exhibited no obvious cytotoxicity to the above mentioned two kinds of cells (cell viability > 80%) even at a concentration of 800 mg L^{-1} (**Figure 3**a and Figure S8 (Supporting Information)). Thereafter, we investigated in vitro photothermal therapy of OVA–ICG nanovaccine. 5 min irradiation with an 808 nm laser (2 W cm^{-2}) of the B16 cells without nanovaccine incubation led to negligible decrease in the cell viability of B16 cells. In contrast, the viability of B16 cells slumped to about 5% after 5 min irradiation with an 808 nm laser (2 W cm^{-2}) and the treatment of OVA–ICG nanovaccine (200 mg L^{-1}) (Figure 3b). The fluorescent images of the B16 cells costained with calcein acetoxymethyl ester and propidium iodide further intuitively proved the outstanding photothermal therapy of OVA–ICG nanovaccine (Figure S9, Supporting Information). These results not only confirm the low cytotoxicity of OVA–ICG, but also reveal the effective photothermal therapy capability of OVA–ICG.

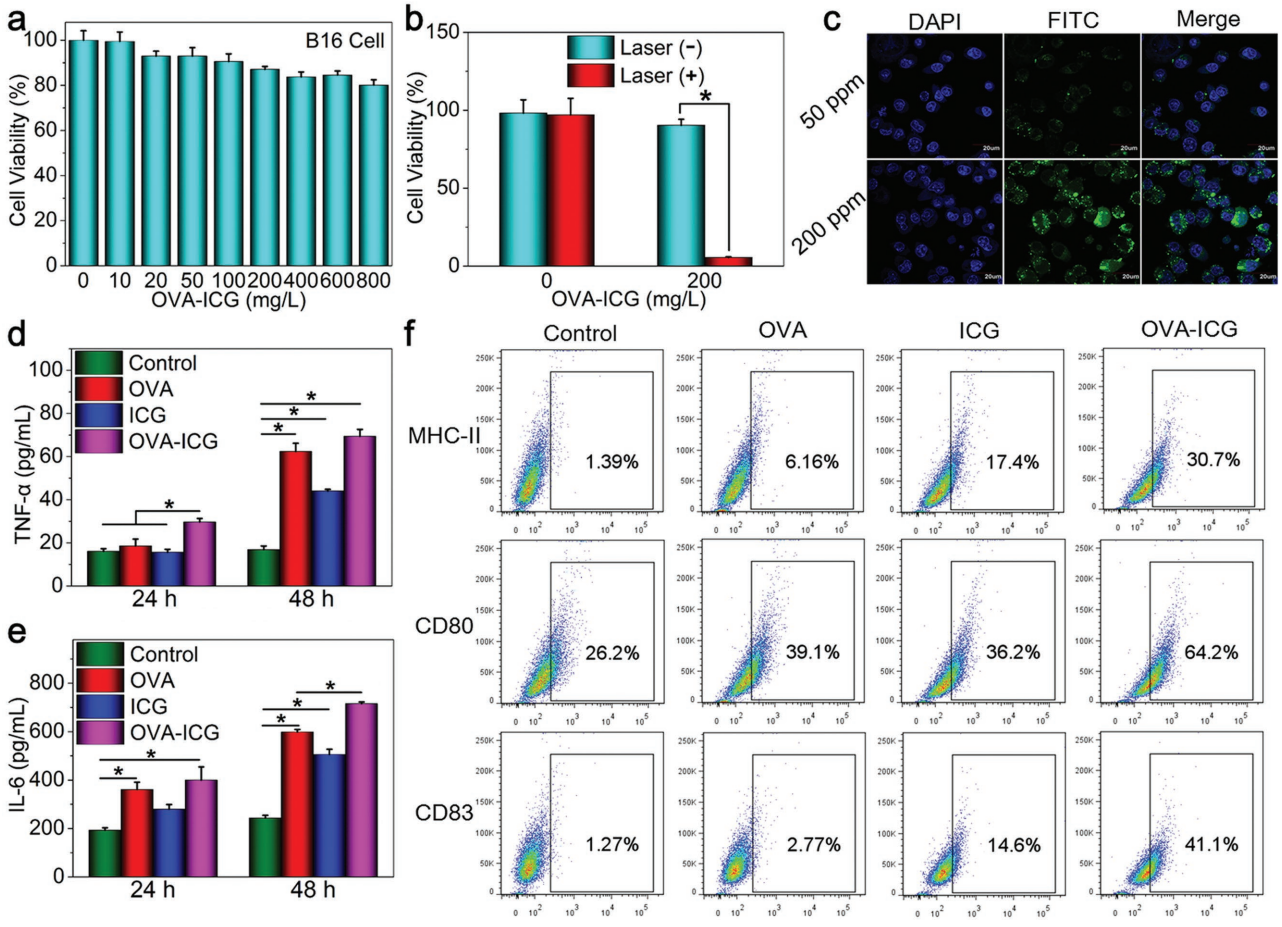

Figure 3. Cytotoxicity, photothermal therapy against B16 cells, and DC activation of OVA–ICG. a) Cell viability of the B16 cells after incubation with different concentrations of OVA–ICG. b) Cell viability of the B16 cells after incubation with OVA–ICG with or without 808 nm laser irradiation (2.0 W cm^{-2}, 5 min). c) Confocal fluorescent images of DC 2.4 cells incubated with different concentrations of FITC-labeled OVA–ICG for 24 h. The amount of d) TNF-α and e) IL-6 in the DC 2.4 cell culture supernatant after incubation with OVA, ICG, and OVA–ICG for 24 and 48 h. f) Expression levels of surface molecules (MHC-II, CD80, and CD83) on DC 2.4 cells after activation with pure OVA, pure ICG, and OVA–ICG nanovaccine.

The excellent biosafety to immune cells encourages us to explore the immune response induced by OVA–ICG nanovaccine. It is well known that antigen present cells (APCs), represented by DC and macrophages, play an irreplaceable role in the adaptive immune defense process in the body. When the antigen is recognized by the immature APCs, they will be phagocytosed by APCs. The APCs get maturity, disposes the antigen, and then present it to the T lymphocytes, resulting in the subsequent cellular immunity or humoral immunity. In the meantime, the mature APCs produce several proinflammation cytokines to facilitate the immune response.[20] Therefore, the phagocytosis of antigen, the maturity of APCs, and the secretion of proinflammation cytokines are essential for the adaptive immune response.

Herein, we choose a universally recognized immature DC cell line, DC 2.4 cells, to investigate the immune activation characteristics of OVA–ICG nanovaccine. The phagocytosis of fluorescein isothiocyanate (FITC)-labeled OVA–ICG nanovaccine into the cytoplasm of DC 2.4 cells was proved by the intracellular green fluorescence in the confocal fluorescent images (Figure 3c). Higher concentration of FITC-labeled OVA–ICG nanoassembly gave rise to more uptake of the nanovaccine. Thereafter, the production of proinflammation cytokines by stimulated DC 2.4 cells was measured via enzyme linked immunosorbent assay. DC 2.4 cells were cultured with OVA, pure ICG, and OVA–ICG nanovaccine for different times (24 and 48 h). The secretion levels of tumor necrosis factor-α (TNF-α) (an important marker in cellular immunity) and interleukin-6 (IL-6) (an important marker in humoral immunity) in the culture supernate were recorded for immunoactivation assessment. Figure 3d reveals that only the OVA–ICG nanovaccine promoted the DC 2.4 cells to secrete significant TNF-α after 24 h incubation. Further increase of the incubation time to 48 h had remarkable increase of TNF-α induced by OVA, ICG, and OVA–ICG nanovaccine compared with the control group. Both OVA and OVA–ICG induced more secretion of IL-6 than the control group, while the secretion levels increased with the stimulating time (Figure 3e). It should be noted that DC 2.4 cells incubated with OVA–ICG secreted more IL-6 than those incubated with pure OVA at the incubation time of 48 h.

Besides phagocytosis and cytokine secretion, the maturity of DC 2.4 after activation also plays a vital role in immune response. The maturity was evaluated based on the expression of special molecules on the cytomembrane of DC 2.4 via the flow cytometry assay. Major histocompatibility complex-II (MHC-II), CD80, and CD83 are important molecules expressed on the cytomembrane of DC. The expression levels of these molecules increased in the meantime when DC was activated. MHC-II can bind antigen and target to T cell receptor on the T cells for antigen presentation, providing the "first signal" for T cell activation. While CD 80 (synergetic with CD86) can recognize and bind to B7 molecules on the T cells, providing the "second signal" for T cell activation. CD83 can modulate the maturity of DC and activation of T cell and B cell and increased expression of CD83 is recognized as an important marker for DC maturation. Encouragingly, OVA, ICG, and OVA–ICG nanovaccine all resulted in remarkably higher expression of MHC-II, CD80, and CD 83 (Figure 3f). The expression levels increased with the concentration of OVA–ICG nanovaccine (Figure S10, Supporting Information). Notably, different from the results of cytokine secretion, OVA–ICG nanovaccine triggered much higher level of surface molecule expression than pure OVA, indicating a more effective activation to DC 2.4 cells. On the other hand, the high expression level of MHC-II and CD 83 induced by pure ICG demonstrated that ICG probably made a synergistic contribution to the maturation of DC 2.4 cells in the immune stimulation of OVA–ICG nanovaccine.[21] All the above results demonstrate that OVA–ICG nanovaccine was efficiently phagocytosed by DC 2.4 cells and promoted the maturity of APCs more powerfully than OVA alone.

We then applied OVA–ICG nanovaccine to photothermal-immunotherapy against melanoma in vivo (**Figure 4**a). B16-bearing mice were intratumorally injected with PBS, ICG, and OVA–ICG nanovaccine individually. All the animal experiments involved in this work were approved by the Tianjin Medical University Animal Care and Use Committee. NIR fluorescent images show impressive fluorescence enhancement in tumor regions after injecting OVA–ICG nanovaccine, enabling monitoring the migration and distribution of the nanovaccine (Figure S11, Supporting Information). For photothermal therapy, the tumors of mice were then exposed to laser irradiation (0.1 W cm^{-2}) for 3 min. The surface temperature of the tumor administrated with ICG and OVA–ICG exhibited a similar enhancement up to about 60 °C (Figure 4b and Figure S12 (Supporting Information)), which is high enough to induce tumor cells apoptosis. In contrast, the surface temperature of the tumor treated with PBS increased to about 47 °C under the same laser exposure due to the black parenchyma of melanoma with light-absorbing ability. However, this insufficient temperature increase did not result in any tumor suppression compared with the negative control group treated with PBS without laser illumination (Figure 4c–e). The tumors treated with OVA–ICG nanovaccine under laser ablation showed the most powerful tumor growth suppression among all the groups owing to the synergistic immunotherapy and photothermal therapy. However, pure ICG led to a weaker tumor inhibition under laser irradiation due to photothermal therapy and probably limited immune response induced by photothermal therapy.[21,22] It is also worth mentioning that only 3 min laser exposure at a very low power (0.1 W cm^{-2}) was required in OVA–ICG nanovaccine-based tumor ablation. The mild illumination conditions effectively avoid the potential photodamage of healthy issues. In addition, the $CD8^+$ cytotoxic T cells in tumors and the specific anti-OVA–immunoglobulin G (IgG) in the serum of mice treated with OVA–ICG nanovaccine (with or without laser irradiation) both exhibited a similar increase (Figures S13 and S14, Supporting Information), demonstrating the reliable antitumoral immunotherapy effect. These results indicated the immunotherapy effect in vivo is mainly induced by OVA–ICG nanovaccine itself, and the limited immune activation induced by photothermal therapy was not sufficient for significant improvement of the immunotherapy effect in our study. Despite the activity of the immune cells suppressed in the tumor microenvironment, the intratumorally injected nanovaccine could permeate into the peritumoral zone to promote the mature of immunocompetent dendritic cells and induce immune response.[23] Moreover, the therapeutic process using OVA–ICG nanovaccine did not need

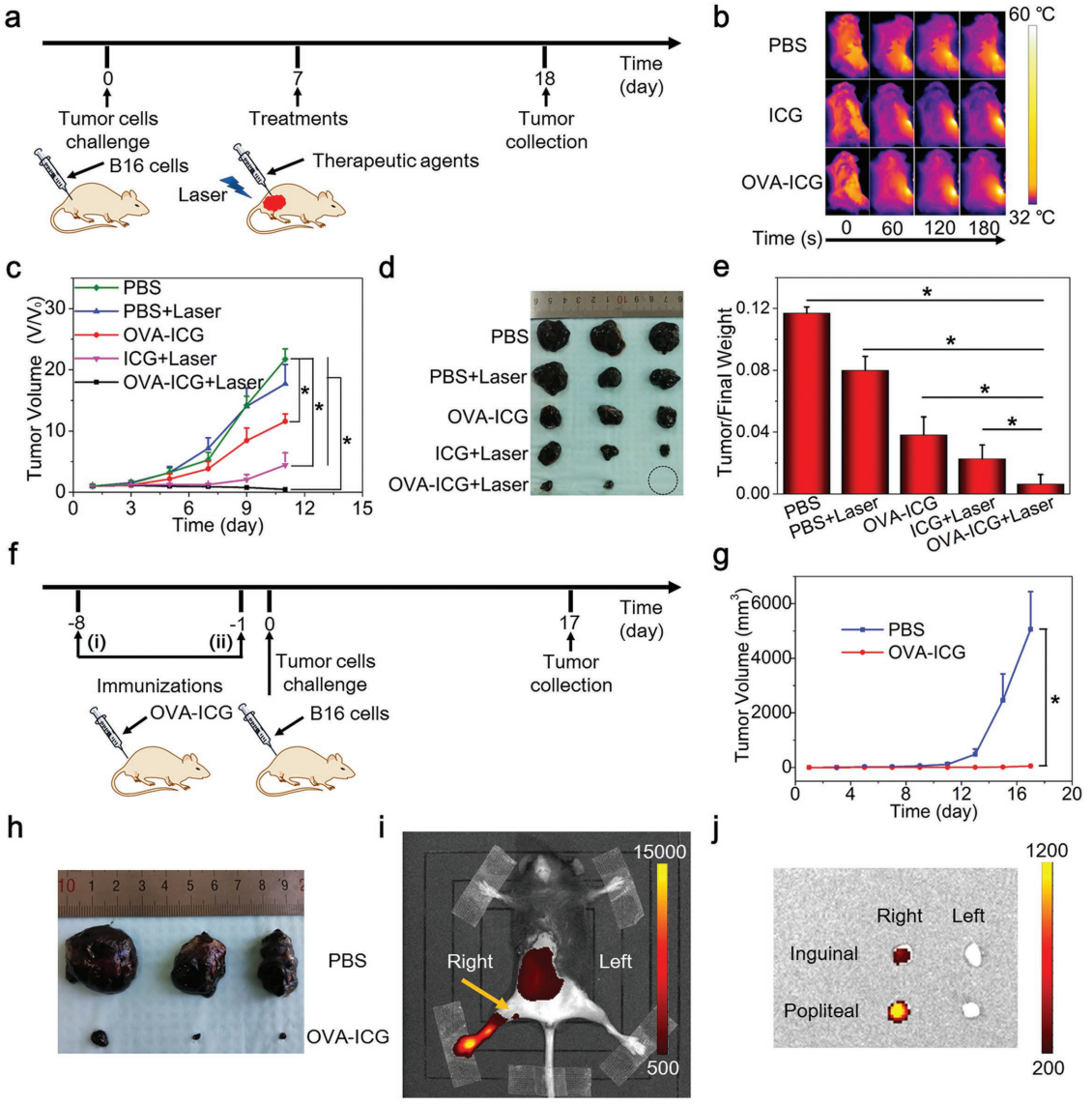

Figure 4. a) Protocol for therapeutic assay. b) IR images of mice during laser irradiation. c) Tumor growth curves of the mice with different treatments. d) Excised melanoma from the mice with different treatments. e) Mean final tumor weight per 100 g of final body weight. f) Protocol for tumor prevention assay. g) Tumor growth curves of the mice treated with PBS or OVA–ICG. h) Excised melanoma from the mice with different treatments. In vivo fluorescence image of i) mouse and j) lymph nodes at 7 h postinjection of OVA–ICG-labeled DC2.4 cells at foot pad (homolateral popliteal lymph node was pointed out by yellow arrow).

any additional immune-boosting treatments, indicating its powerful immunotherapy efficacy via only a single administration. Besides, the OVA–ICG nanovaccine-based therapy did not lead to notable body weight decline (Figure S15, Supporting Information) and histopathologic changes of vital organs in the body (Figure S16, Supporting Information), showing a good biocompatibility in vivo.

Figure 4f illustrates the protocol for tumor prevention with OVA–ICG nanovaccine. The mice were treated with the immunization of OVA–ICG or PBS twice to evoke immune activation before tumor cells challenge. OVA–ICG immunized mice exhibited impressive melanoma suppression ability compared with PBS treated group as the former average tumor size was almost 100 times smaller than the latter one (Figure 4g,h). When the melanoma-specific antigen OVA was recognized by the APCs in the subcutaneous tissues, the APCs were stimulated to present the antigen to the T cells. Subsequently, a series of adaptive immune activations and immunologic memory was generated. Once B16 cells (overexpressing OVA) were transplanted into immunized mice again, the immune system was immediately evoked to eliminate the B16 cells. Therefore, OVA–ICG nanovaccine not only enables robust combined photothermal therapy and immunotherapy, but also serves as a robust nanovaccine for tumor prevention.

Besides impressing synergistic antitumor and tumor prevention performance, strong NIR fluorescence and effective DC labeling and stimulation endow OVA–ICG nanovaccine with great potential in activated DC tracking in vivo. In DC-based

immunotherapy, the migration of antigen-loaded DCs from injection sites to draining lymph nodes through lymphatic vessels is essential for arousing immune system to destroy tumors. To investigate DC tracking ability, OVA–ICG-labeled DC 2.4 cells were injected into the right foot pad of C57BL/6 mice to track the progress of DC migration with an in vivo fluorescent imaging system. Intense fluorescence of OVA–ICG-labeled DC 2.4 cells was observed in the popliteal lymph node at 7 h postinjection, while weak fluorescence was also seen in the homolateral inguinal lymph node (Figure 4i,j). However, contralateral lymph nodes showed no fluorescent signal. These results indicate the whole migration process of DC 2.4 cells from initial injection site to the draining lymph node via lymphatic vessels was sensitively tracked using OVA–ICG nanovaccine.

In summary, to overcome the drawbacks of limited antigen loading efficiency, low yield, tedious manufacture, and systemic toxicity in current antigen-encapsulated multifunctional nanovaccines, we have reported an antigen-directed synthesis strategy for building multifunctional nanovaccine with ultrahigh antigen loading efficiency for tumor photothermal-immunotherapy. The antigen is employed as a natural carrier to load the theranostic agent. The model OVA–ICG nanovaccine was fabricated in aqueous solution at room temperature via an extremely facile mixing method without the need of toxic agents and inert gas protection, and is the simplest nanovaccine so far. The fabricated nanovaccine exhibits impressive advantages of antigen loading efficiency of 80.8%, high yield (>90%), intense NIR absorption and fluorescence, excellent reproducibility, admirable aqueous solubility and stability, and favorable biocompatibility. The robust and safe nanovaccine enables high-efficient stimulation, sensitive labeling/tracking of DC cells, synergistic photothermal-immunotherapy against tumors, and powerful tumor prevention. We believe that the proposed antigen-directed synthesis strategy paves a facile and robust way for large-scale and reproducible fabrication of multifunctional therapeutic nanovaccines with high antigen loading efficiency using various antigens and theranostic agents.

Supporting Information

Supporting Information is available from the Wiley Online Library or from the author.

Acknowledgements

J.P., Y.W., and C.Z. contributed equally to this work. This work was supported by the National Natural Science Foundation of China (Grants 21435001, 21405112, 81401471), the Tianjin City High School Science & Technology Fund Planning Project (Grant 20140120), and the China Postdoctoral Science Foundation (Grant 2015M581306).

Conflict of Interest

The authors declare no conflict of interest.

Keywords

antigen, dendritic cells, multifunctional nanovaccines, photothermal-immunotherapy, tumor prevention

Received: August 5, 2017
Revised: November 1, 2017
Published online:

[1] R. L. Siegel, K. D. Miller, A. Jemal, *CA: Cancer J. Clin.* **2015**, *65*, 5.
[2] C. E. Meacham, S. J. Morrison, *Nature* **2013**, *501*, 328.
[3] a) I. Mellman, G. Coukos, G. Dranoff, *Nature* **2011**, *480*, 480; b) R. D. Schreiber, L. J. Old, M. J. Smyth, *Science* **2011**, *331*, 1565; c) W. Jiang, C. A. von Roemeling, Y. Chen, Y. Qie, X. Liu, J. Chen, B. Y. S. Kim, *Nat. Biomed. Eng.* **2017**, *1*, 0029.
[4] a) J. G. van den Boorn, G. Hartmann, *Immunity* **2013**, *39*, 27; b) P. L. Lollini, F. Cavallo, P. Nanni, G. Forni, *Nat. Rev. Cancer* **2006**, *6*, 204; c) M. S. Goldberg, *Cell* **2015**, *161*, 201.
[5] E. Yuba, N. Tajima, Y. Yoshizaki, A. Harada, H. Hayashi, K. Kono, *Biomaterials* **2014**, *35*, 3091.
[6] M. Luo, H. Wang, Z. Wang, H. Cai, Z. Lu, Y. Li, M. Du, G. Huang, C. Wang, X. Chen, M. R. Porembka, J. Lea, A. E. Frankel, Y. X. Fu, Z. J. Chen, J. Gao, *Nat. Nanotechnol.* **2017**, *12*, 648.
[7] Y. Tao, Y. Zhang, E. Ju, H. Ren, J. Ren, *Nanoscale* **2015**, *7*, 12419.
[8] S. B. Stephan, A. M. Taber, I. Jileaeva, E. P. Pegues, C. L. Sentman, M. T. Stephan, *Nat. Biotechnol.* **2015**, *33*, 97.
[9] C.-T. Tsao, F. M. Kievit, A. Ravanpay, A. E. Erickson, M. C. Jensen, R. G. Ellenbogen, M. Zhang, *Biomacromolecules* **2014**, *15*, 2656.
[10] J. Kim, W. A. Li, Y. Choi, S. A. Lewin, C. S. Verbeke, G. Dranoff, D. J. Mooney, *Nat. Biotechnol.* **2015**, *33*, 64.
[11] D. Ni, S. Qing, H. Ding, H. Yue, D. Yu, S. Wang, N. Luo, Z. Su, W. Wei, G. Ma, *Adv. Sci.* **2017**, *4*, 1700083.
[12] a) T. H. Schreiber, L. Raez, J. D. Rosenblatt, E. R. Podack, *Semin. Immunol.* **2010**, *22*, 105; b) K. Shao, S. Singha, X. Clemente-Casares, S. Tsai, Y. Yang, P. Santamaria, *ACS Nano* **2015**, *9*, 16.
[13] a) D. J. Irvine, M. C. Hanson, K. Rakhra, T. Tokatlian, *Chem. Rev.* **2015**, *115*, 11109; b) M. Luo, L. Z. Samandi, Z. Wang, Z. J. Chen, J. Gao, *J. Control. Release* **2017**, *263*, 200; c) G. Zhu, F. Zhang, Q. Ni, G. Niu, X. Chen, *ACS Nano* **2017**, *11*, 2387.
[14] a) M. Vanneman, G. Dranoff, *Nat. Rev. Cancer* **2012**, *12*, 237; b) C. Wang, W. Sun, Y. Ye, Q. Hu, H. N. Bomba, Z. Gu, *Nat. Biomed. Eng.* **2017**, *1*, 0011.
[15] a) D. Jaque, L. Martinez Maestro, B. del Rosal, P. Haro-Gonzalez, A. Benayas, J. L. Plaza, E. Martin Rodriguez, J. Garcia Sole, *Nanoscale* **2014**, *6*, 9494; b) Q. Chen, J. Wen, H. Li, Y. Xu, F. Liu, S. Sun, *Biomaterials* **2016**, *106*, 144.
[16] a) L. Guo, D. D. Yan, D. Yang, Y. Li, X. Wang, O. Zalewski, B. Yan, W. Lu, *ACS Nano* **2014**, *8*, 5670; b) Q. Chen, L. Xu, C. Liang, C. Wang, R. Peng, Z. Liu, *Nat. Commun.* **2016**, *7*, 13193.
[17] a) Q. Chen, Z. Liu, *Adv. Mater.* **2016**, *28*, 10557; b) W. Yang, W. Guo, J. Chang, B. Zhang, *J. Mater. Chem. B* **2017**, *5*, 401.
[18] a) J. P. Xie, Y. G. Zheng, J. Y. Ying, *J. Am. Chem. Soc.* **2009**, *131*, 888; b) N. Ma, A. F. Marshall, J. H. Rao, *J. Am. Chem. Soc.* **2010**, *132*, 6884; c) B. B. Zhang, H. T. Jin, Y. Li, B. D. Chen, S. Y. Liu, D. L. Shi, *J. Mater. Chem.* **2012**, *22*, 14494; d) S.-K. Sun, L.-X. Dong, Y. Cao, H.-R. Sun, X.-P. Yan, *Anal. Chem.* **2013**, *85*, 8436; e) P. Huang, P. Rong, A. Jin, X. Yan, M. G. Zhang, J. Lin, H. Hu, Z. Wang, X. Yue, W. Li, G. Niu, W. Zeng, W. Wang, K. Zhou, X. Chen, *Adv. Mater.* **2014**, *26*, 6401; f) Z. H. Sheng, D. H. Hu, M. B. Zheng, P. F. Zhao, H. L. Liu, D. Y. Gao, P. Gong, G. H. Gao, P. F. Zhang, Y. F. Ma, L. T. Cai, *ACS Nano* **2014**, *8*, 12310; g) Q. Chen, C. Liang, C. Wang, Z. Liu, *Adv. Mater.* **2015**, *27*, 903; h) Y. Wang, T. Yang,

H. Ke, A. Zhu, Y. Wang, J. Wang, J. Shen, G. Liu, C. Chen, Y. Zhao, H. Chen, *Adv. Mater.* **2015**, *27*, 3874; i) C. Zhang, Y.-Y. Fu, X. Zhang, C. Yu, Y. Zhao, S.-K. Sun, *Dalton Trans.* **2015**, *44*, 13112; j) F. Mao, L. Wen, C. Sun, S. Zhang, G. Wang, J. Zeng, Y. Wang, J. Ma, M. Gao, Z. Li, *ACS Nano* **2016**, *10*, 11145; k) Y. Wang, Y. Y. Wu, Y. J. Liu, J. Shen, L. Lv, L. B. Li, L. C. Yang, J. F. Zeng, Y. Y. Wang, L. S. W. Zhang, Z. Li, M. Y. Gao, Z. F. Chai, *Adv. Funct. Mater.* **2016**, *26*, 5335; l) T. Yang, Y. Wang, H. Ke, Q. Wang, X. Lv, H. Wu, Y. Tang, X. Yang, C. Chen, Y. Zhao, H. Chen, *Adv. Mater.* **2016**, *28*, 5923; m) W. T. Yang, W. S. Guo, W. J. Le, G. X. Lv, F. H. Zhang, L. Shi, X. L. Wang, J. Wang, S. Wang, J. Chang, B. B. Zhang, *ACS Nano* **2016**, *10*, 10245; n) C. Zhang, L. Zhou, J. Zhang, Y.-Y. Fu, X. Zhang, C. Yu, S.-K. Sun, X.-P. Yan, *Nanoscale* **2016**, *8*, 16204; o) J. B. Pan, Y. Q. Wang, H. Y. Pan, C. Zhang, X. G. Zhang, Y. Y. Fu, X. J. Zhang, C. S. Yu, S. K. Sun, X. P. Yan, *Adv. Funct. Mater.* **2017**, *27*, 1603440.

[19] a) X. F. Zhang, L. Chen, Q. F. Yang, Q. Li, X. R. Sun, H. B. Chen, G. Yang, Y. L. Tang, *Luminescence* **2015**, *30*, 1176; b) X. Li, Y. Yan, *J. Fluoresc.* **2017**, *27*, 213.

[20] a) K. Palucka, J. Banchereau, *Nat. Rev. Cancer* **2012**, *12*, 265; b) N. P. Restifo, M. E. Dudley, S. A. Rosenberg, *Nat. Rev. Immunol.* **2012**, *12*, 269; c) P. G. Coulie, B. J. Van den Eynde, P. van der Bruggen, T. Boon, *Nat. Rev. Cancer* **2014**, *14*, 135.

[21] C. Wang, L. Xu, C. Liang, J. Xiang, R. Peng, Z. Liu, *Adv. Mater.* **2014**, *26*, 8154.

[22] F. Zhou, X. Li, M. F. Naylor, T. Hode, R. E. Nordquist, L. Alleruzzo, J. Raker, S. S. K. Lam, N. Du, L. Shi, X. Wang, W. R. Chen, *Cancer Lett.* **2015**, *359*, 169.

[23] a) S. Wang, Y. Chen, X. Li, W. Gao, L. Zhang, J. Liu, Y. Zheng, H. Chen, J. Shi, *Adv. Mater.* **2015**, *27*, 7117; b) K. Hayashi, W. Sakamoto, T. Yogo, *Adv. Funct. Mater.* **2016**, *26*, 1708; c) W. Zhao, J. Hu, W. Gao, *ACS Appl. Mater. Interfaces* **2017**, *9*, 23528.